RESEARCH ARTICLE | DECEMBER 02 2024

# First-principles study of the electronic structure, $Z_2$ invariant, and quantum oscillation in the kagome material $CsV_3Sb_5$

Shalika R. Bhandari ; Mohd Zeeshan; Vivek Gusain ; Keshav Shrestha; D. P. Rai



*APL Quantum* 1, 046118 (2024)
https://doi.org/10.1063/5.0232167

# First-principles study of the electronic structure, $Z_2$ invariant, and quantum oscillation in the kagome material $CsV_3Sb_5$

Cite as: APL Quantum 1, 046118 (2024); doi: 10.1063/5.0232167
Submitted: 5 August 2024 • Accepted: 30 October 2024 •
Published Online: 2 December 2024



Shalika R. Bhandari,[1,2,a] Mohd Zeeshan,[3] Vivek Gusain,[3] Keshav Shrestha,[4] and D. P. Rai[5,b]

## AFFILIATIONS

[1] Department of Physics, Bhairahawa Multiple Campus, Tribhuvan University, Siddarthanagar 32900, Rupandehi, Nepal
[2] Leibniz Institute for Solid State and Materials Research, IFW Dresden, Dresden 01609, Germany
[3] Department of Physics, Indian Institute of Technology, Hauz Khas, New Delhi 110016, India
[4] Department of Chemistry and Physics, West Texas A and M University, Canyon, Texas 79016, USA
[5] Department of Physics, Mizoram University, Aizawl 796004, India

[a] E-mail: shalikram.bhandari@bmc.tu.edu.np
[b] Author to whom correspondence should be addressed: dibyaprakashrai@gmail.com

## ABSTRACT

This work presents a detailed study of the electronic structure, phonon dispersion, $\mathbf{Z}_2$ invariant calculation, and Fermi surface of the newly discovered kagome superconductor $CsV_3Sb_5$, using density functional theory. The phonon dispersion in the pristine state reveals two negative modes at the M and L points of the Brillouin zone, indicating lattice instability. $CsV_3Sb_5$ transitions into a structurally stable $2 \times 2 \times 1$ charge density wave (CDW) phase, confirmed by positive phonon modes. The electronic band structure shows several Dirac points near the Fermi level, with a narrow gap opening due to spin–orbit coupling (SOC), although the effect of SOC on other bands is minimal. In the pristine phase, this material exhibits a quasi-2D cylindrical Fermi surface, which undergoes reconstruction in the CDW phase. We calculated quantum oscillation frequencies using Onsager's relation, finding good agreement with experimental results in the CDW phase. To explore the topological properties of $CsV_3Sb_5$, we computed the $\mathbf{Z}_2$ invariant in both pristine and CDW phases, resulting in a value of $(\nu_0; \nu_1\nu_2\nu_3) = (1; 000)$, suggesting the strong topological nature of this material. Our detailed analysis of phonon dispersion, electronic bands, Fermi surface mapping, and $\mathbf{Z}_2$ invariant provides insights into the topological properties, CDW order, and unconventional superconductivity in $AV_3Sb_5$ (A = K, Rb, and Cs).





## I. INTRODUCTION

In recent years, kagome metals have garnered significant research interest due to their distinctive quantum characteristics owing to the unique lattice structure that resembles a Japanese bamboo basket. The kagome lattice is composed of a two-dimensional network of corner-sharing triangles and hexagons. A series of layered kagome metals $AV_3Sb_5$ (A = K, Rb, and Cs) are found with various intriguing complex properties such as charge density wave (CDW) order, superconductivity (SC), Fermi crossing, band topology with anomalous Hall effect (AHE), flatbands across the Brillouin zone, and van Hove singularities (VHSs).[1–8] These properties originate from the inherent characteristics of the kagome lattice: spin frustration, flatbands, Dirac cones, and VHSs at various locations. So far, the series of $AV_3Sb_5$ is being synthesized, modeled, and characterized by a number of theoretical[9–13] and experimental groups.[14–20] Our literature survey on Kagome materials indicates that at 80–100 K, CDW arises from hexagonal $AV_3Sb_5$ (A = K, Rb, and Cs) compounds with stacked vanadium kagome layers. The CDW phases of $AV_3Sb_5$ are found to exhibit superconducting behavior with transition temperature ($T_c$) = 0.9–2.5 K.[5,8,21] With the application of pressure on $AV_3Sb_5$, two superconducting domes have appeared with enhanced $T_c$ and no sign of a structural phase transition.[22–25] In addition to the translational symmetry break-

ing in the CDW phase, the rotation and time-reversal symmetry breaking also appeared on cooling down toward $T_c$.[26–28] CDW was recently found in the bilayer kagome metal $ScV_6Sn_6$, in which the V atoms form kagome bilayers,[21,29] and also in the kagome metal FeGe, which develops antiferromagnetic (AFM) order and results in an improvement of the ordered moment.[30,31] CDW in the kagome metal FeGe offers additional flexibility for studying the interaction between magnetism and CDW. Despite their exceptional similarity, it has been found that the electronic structure of the Cs compound is very different from the K and Rb materials in $AV_3Sb_5$.[32]

In most studies, the majority of research on the kagome materials is focused on the SC and its relationship to CDW. However, we have observed the limited reports on the topology, $\mathbf{Z}_2$ invariant, and Fermi-surface calculations. In the series of $AV_3Sb_5$ (A = K, Rb, and Cs), we are particularly interested in $CsV_3Sb_5$ due to its topologically non-trivial band structure with many Dirac-like bands crossing near the Fermi level, the highest superconducting $T_c$, and the non-zero topological invariant $\mathbf{Z}_2$, suggesting a strong candidate for further topological investigation.[20,24,33,34]

There are various assumptions on the origin of the CDW state in the $AV_3Sb_5$ series. Some report that CDW state is induced by the Peierls instability related to the Fermi surface nesting and phonon softening,[35,36] while other main views on the origin of CDW state formation in the $AV_3Sb_5$ series are exciton condensation,[37,38] momentum-dependent EPC,[39,40] saddle-point nesting,[41] and Jahn–Teller-like instability.[42] However, solid knowledge of the lattice and electronic properties of the CDW state is still missing to understand the superconductivity and topology, which calls for future studies. In this study, we have presented first principles electronic calculations on the pristine and CDW states of $CsV_3Sb_5$, providing a thorough understanding of the experimental work. We report that the CDW transition is related to breathing-phonon modes of the kagome lattice and mediated by the Fermi surface instability. To confirm the topologically non-trivial band structure, we report Wannier centers on $CsV_3Sb_5$ for pristine and CDW phases, which have been presented for the first time to our knowledge.

## II. COMPUTATIONAL DETAILS AND NUMERICAL SOFTWARE

Two computational codes, such as WIEN2k[43] and FPLO (full-potential local-orbital)[44,45] has been used for the electronic structure, $\mathbf{Z}_2$ invariant, and Fermi surface calculations, as reported recently.[46–48] Vienna *Ab Initio* Simulation Package (VASP) has been used for phonon dispersion calculation by using the finite displacement method (FDM).[49] We constructed a 3 ×3× 2 (162 atoms) and 2 ×2× 2 (288 atoms) supercell for pristine and Inverse Star of David (ISD) structures, respectively, to obtain the phonon dispersion curves using the phonopy package.[50] The phonon dispersion curves are obtained by solving the following equation:

$$\sum_{\beta\tau'} D^{\alpha\beta}_{\tau\tau'}(\mathbf{q})\gamma^{\beta\tau'}_{\mathbf{q}j} = \omega^2_{\mathbf{q}j}\gamma^{\alpha\tau}_{\mathbf{q}j}, \tag{1}$$

where the indices $\tau, \tau'$ represent the atoms, $\alpha, \beta$ are the Cartesian coordinates, $\mathbf{q}$ is a wave vector, $j$ is a band index, $D(\mathbf{q})$ represents the dynamical matrix, $\omega$ signifies the corresponding phonon frequency, and $\gamma$ is the polarization vector.

All the codes are based on the full-potential linearized augmented plane wave method within a framework of density functional theory (DFT). All electrons were treated within the standard generalized gradient approximation (PBE-GGA) using the parameterization of Perdew, Burke, and Ernzerhof (PBE-96).[51] The outermost electron configurations taken for the calculations are $5s^25p^66s^1$ for Cs, $3s^23p^63d^34s^2$ for V, and $4d^{10}5s^25p^3$ for Sb, respectively. The electronic bands derived from Cs-5*p*, V-3*d*, and Sb-5*p* are fitted to a tight-binding Hamiltonian as in Fig. 4(a) by using the maximally projected Wannier functions method as implemented in FPLO code to obtain Hamiltonian data (see Fig. 3 in the supplementary material for the ISD phase). The Wannier fitting was done using the pyfplo[44] module of the FPLO package. The Hamiltonian data were used in the Fermi surface and $\mathbf{Z}_2$ invariant calculations. The four-component Dirac equation was solved for full-relativistic calculations. The first Brillouin zone was integrated within a Bloch corrected linear tetrahedron method using a $12 \times 12 \times 12$ **k**-point mesh for the pristine and an $18 \times 18 \times 16$ **k**-point mesh for the CDW state. The self-consistent calculations were carried out with a spin–orbit coupling (SOC). We have considered a $2 \times 2 \times 1$ superlattice for CDW phase calculation due to the presence of weak interlayer interaction. The Fermi surfaces were generated using 5000 **k**-points, which produces a dense **k**-point mesh of $28 \times 28 \times 26$. From our DFT calculation, $CsV_3Sb_5$ is found to be stable with the lowest energy in a non-magnetic state and exhibit metallic behavior, consistent with the experimental report.[1,52]

## III. RESULTS AND DISCUSSION

The crystal structure of $CsV_3Sb_5$ with the mixture of triangle and layered hexagonal lattices forms the intermetallic kagome networks,[28,53] as shown in Figs. 1(a) and 1(b). In the 2D kagome net of V atoms of $CsV_3Sb_5$, Sb is intercalated by the triangular lattices and Cs atoms at the corner of the cube, forming the layered hexagonal-prismatic symmetry with the space group *P6/mmm* (191) as shown in Figs. 1(a)–1(c). The kagome net of vanadium is interwoven with a simple hexagonal net made up of Sb1 sites. From a space-filling point of view, the Sb1 atoms fill up the natural gap created in the kagome plane. Structural optimization of the lattice parameters and atomic positions on the experimentally obtained[1,20] structure was performed until the forces on each atom were less than 0.14 meV/Å. Optimized lattice parameters opted for the calculation are $a = b = 5.43$ Å, $c = 9.21$ Å, and $\Gamma = 120°$. The variation of $a$ and $c$ with the application of pressure for both the pristine and ISD phases is presented in Table I in the supplementary material.

### A. Phonon dispersion

The phonon dispersion relations of the pristine and CDW states of $CsV_3Sb_5$ at ambient pressure have been calculated from the *ab initio* FDM method and shown in Figs. 1(d)–1(g). In Fig. 1(d), we have found two negative energies of the soft acoustic phonon modes (two imaginary phonon frequencies) at the first Brillouin zone around M and L points. This finding is consistent with the previous reports[5,54,55] and indicates a strong instability. Such instability plays an important role in driving the CDW transition. The

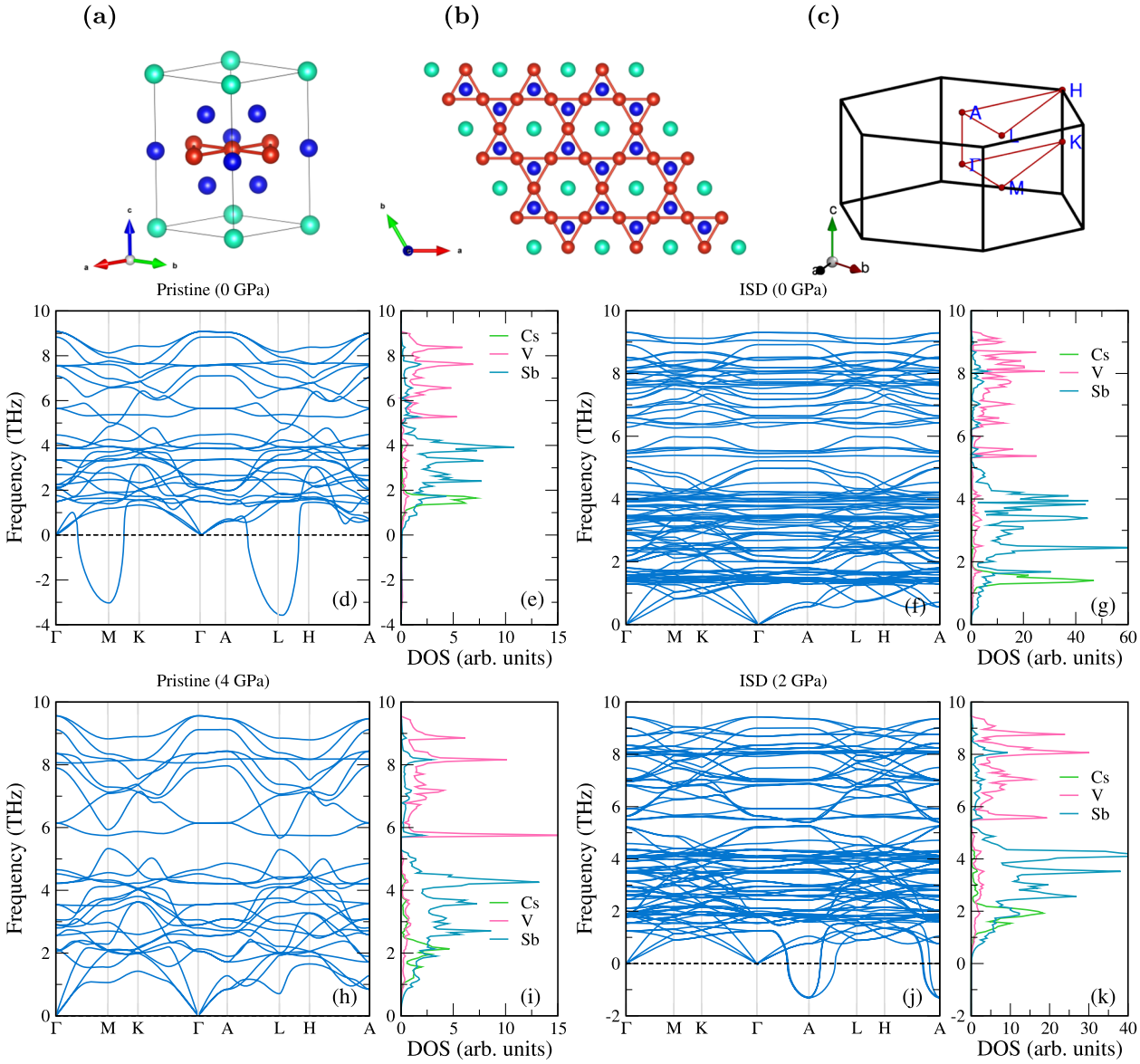


**FIG. 1.** (a) A unit cell of $CsV_3Sb_5$. (b) Top view of $CsV_3Sb_5$ layer showing kagome layer of V atoms. Atoms represented by cyan, red, and blue denote Cs, V, and Sb, respectively. (c) Brillouin zone of the space group *P6/mmm* (191) and the main symmetry directions. (d) Phonon dispersions band structure and (e) density of states of the pristine phase of $CsV_3Sb_5$ at 0 GPa. Imaginary (negative) phonon frequency in (d) corresponds to the breathing mode of the kagome lattice. Such breathing instability is related to CDW distortions. Breathing out and breathing in lead to two different structures in the CDW phase. (f) Phonon dispersions band structure and (g) density of states of $2 \times 2 \times 2$ ISD state of $CsV_3Sb_5$ at 0 GPa. (h) Phonon dispersions band structure and (i) density of states of $2 \times 2 \times 2$ pristine state of $CsV_3Sb_5$ at 4 GPa. (j) Phonon dispersions band structure and (k) density of states of $2 \times 2 \times 2$ ISD state of $CsV_3Sb_5$ at 2 GPa.

structural instabilities led by these soft modes, the Star of David (SoD) and tri-hexagonal (TrH) [also named the inverse Star of David (ISD)] structure configurations, are proposed to be the likely candidates for CDW structures. In Fig. 1(d), the L-point soft mode suggests the presence of a $2 \times 2 \times 2$ reconstruction, whereas the M-point soft mode is associated with a breathing phonon of V atoms in the kagome lattice. Both the symmetry points have the same in-plane projection, which is equivalent to the vector of the CDW order. Moving to a $2 \times 2$ supercell ISD structure, the imaginary frequencies disappear in the phonon band spectra, as shown in Fig. 1(f). The ISD structure forms by an inverse deformation when V1 (V2) atoms move away (toward) the center, which is comparable to the well-known CDW effect in 1T $TaS_2$.[56] Breathing in and out leads to two distinct structures, and breathing deformation reduces the

total energy; hence, the ISD structure achieves a dynamically stable structure.

For the confirmation of its stability in the ground state, we also checked the ground state energies of SD and ISD structures. On comparing the ground state energies, we found that, in the 2 × 2 × 2 CDW, the SD phase has higher energy in its ground state and relaxes to the ISD structure spontaneously. A recent study on the stability of CDW surfaces using a slab model has also shown that the ISD phase is more stable with the Cs termination.[5,57] Therefore, the ISD structure is energetically favored over the SD.

We have also studied the pressure effect on phonon dispersion for low range pressure up to 6 GPa for both the pristine and CDW phases. Phonon dispersion for both states for 1–6 GPa has been presented in the supplementary material (Figs. 1 and 2 in the supplementary material). For the pristine phase, the imaginary phonon modes at M and L points gradually decrease up to 3 GPa, and they completely vanish at and above 4 GPa (Fig. 1 in the supplementary material). It shows complete suppression of the CDW phase with increasing pressure, which agrees with the earlier experimental report.[58] In the case of the CDW state, interestingly imaginary phonon modes appear at 2 GPa, and they vanish at and above 3 GPa (Fig. 2 in the supplementary material). The imaginary phonon at 2 GPa is supposed to be due to the structural distortion, which mainly consists of the movement of V atoms in the *ab* plane. Some studies propose electronic correlations at ambient pressure and CDW fluctuations around 2 GPa to be the main driving force behind the formation of Cooper pairs.[12,59,60] This imaginary phonon mode in the CDW phase also predicts the suppression of the CDW phase at 2 GPa, which needs further experimental examination.

### B. Crystal, electronic structure, and Fermi surface

The CDW state is found to be three dimensional (3D) and modulated along the c-axis. This modulation, which is still in debate, is either 2 × 2 × 2 or 2 × 2 × 4 for the $AV_3Sb_5$ series, with 2 × 2 × 2 reported for $KV_3Sb_5$, and both 2 × 2 × 2 and 2 × 2 × 4 reported for $CsV_3Sb_5$.[28,61,62] The 2 × 2 × 2 CDW has a similar electronic structure as the 2 × 2 × 1 one because of the weak interlayer interaction.[5] For simplicity of analysis and computational capacity, we focus only on the in-plane distortion, 2 × 2 × 1 superlattice (i.e., 2 × 2) CDW phase in the following discussions.

The total and partial density of states (DOS) (see Fig. 3 in the supplementary material) and orbital-resolved band structure of $CsV_3Sb_5$ for pristine and CDW phases within GGA + SOC are shown in Fig. 2. The major contribution to the total DOS around $E_F$ is mainly from V-3*d* and Sb-5*p* orbitals. Here, the Fermi surface lies within the vanadium *d*-orbital. The DOS exhibits a local minimum near $E_F$, an indication of a semi-metal. The calculated orbital-resolved band structure of normal-state $CsV_3Sb_5$ shows that there are two bands (bands 67 and 68) crossing the $E_F$. The two bands that cross the $E_F$ around the Γ and A points are primarily provided by the out-of-plane orbitals of Sb-*pz*, and the bands near the M and L points are dominated by the out-of-plane orbitals of V-$d_{xz}/d_{yz}$. In addition, we detect several Dirac points close to the $E_F$ that are dominated by the in-plane orbitals of V-$d_{xy}$ / $d_{x^2-y^2}$ [Fig. 2(b)], agreeing well with the previous DFT report.[5,6] Aside from a set of dispersive bands around Γ and A, the majority of band crossings are caused by Dirac-like features at H, K, L, and even at H–A. A fascinating aspect of the band diagram can be found if we look at the features at the K and H points. These are not isolated Dirac cones; when we look at the dispersion along K–H, it has been found that the features are linked together, developing a conical valley. The strength of the related interlayer coupling influences the bulk band structure. In $CsV_3Sb_5$, the interlayer coupling is found to be weak, resulting in a quasi two-dimensional (2D) band structure. In the band structure, four VHS points formed by vanadium 3*d* orbitals around the M point near the $E_F$ are identified, which are in agreement with earlier work.[1,2,25,32,63] Three of them are near the $E_F$, and another is just below the $E_F$ around M point. VHSs, with their large density of states, bring about a significant decrease in the local Coulomb interaction and also play an important role in the different Fermi surface instabilities, which are supported by the angle-resolved photoemission spectroscopy (ARPES) experiment.[32,63]

A comparison of band structure in the pristine and charge density wave (CDW) states is shown in Figs. 2(c) and 2(f), respectively. The general characteristics of bands in the CDW state, which has a large number of bands due to supercell structure, are unchanged for those that are contributed from Sb-orbitals near Γ points. Dirac cones at K and H points of BZ below $E_F$ remain unbroken in both states [Figs. 2(c) and 2(f)], which are consistent with the earlier report.[5] The bands near BZ, which are contributed by V orbitals, have been changed in the CDW state and with the application of SOC, which can be seen at M and L symmetry points. It is due to 2 × 2× 1 distortion on the V kagome lattice and the effect of SOC in 3*d* orbitals. These characters can be rationalized by the fact that bands close to the $E_F$ are mostly contributed by V. It has been found from the calculation that SOC affects some of the Sb-*p* bands, and it also opens a small gap at the Dirac point near K [Fig. 2(c)], but it does not alter the location of the VHS points, which are in agreement with previous work.[64] Here, we investigate that both the pristine and CDW states have a topologically non-trivial band structure with a non-zero $\mathbf{Z}_2$ topological invariant for the band near $E_F$ (see detail in Sec. III). From DFT calculations, the topological invariant $\mathbf{Z}_2$ for $CsV_3Sb_5$ is found to be $(\nu_0; \nu_1\nu_2\nu_3) = (1; 000)$. This suggests a $\pi$-Berry phase accumulated along the cyclotron orbit, which is consistent with the cylindrical-shaped Fermi surface as in Fig. 3.

The Fermi surface (FS) of the $CsV_3Sb_5$ kagome compound for pristine and ISD phases from the relevant band structures has been presented in Fig. 3. Both electron and hole-like sheets have been found in the topology, which has an important contribution while identifying the sign of the Hall coefficient of a material.[65] In the pristine state, a cylinder-like FS is centered around the Γ-point (or along the Γ-A path) for band 67 contributed by Sb-*Pz* states, suggesting a 2D nature of the electronic properties. A big and complex electron/hole-like hexagonal sheet (FSs) contributed by V-*d* states centered around the Γ-point is also obtained. A much smaller FSs hole-like and electron-like FS sheet appears along the Γ-M path and near K-points, respectively, that are contributed by V-*d* states for band 68.

On the other hand, the 2 × 2 ISD CDW distortion modifies the FSs. The Fermi surface becomes reconstructed by the CDW pattern. The bands near the BZ boundary at M and K are strongly modified, including the large hexagonal FS and small FSs. Different from V-*d* driven FSs, the cylinder-like FSs from Sb-*Pz* are marginally affected by the CDW deformation, as shown in Fig. 3. Because the

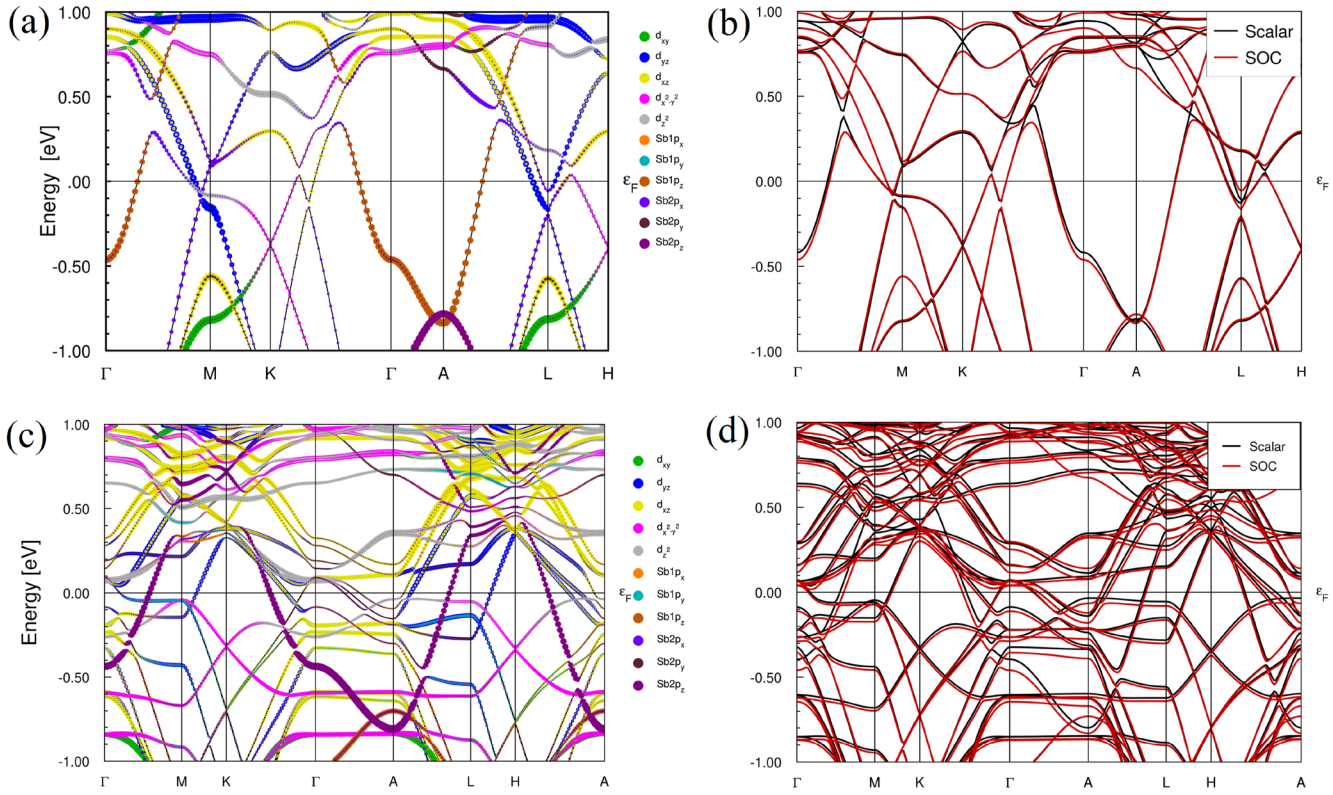


**FIG. 2.** DFT calculated (a) orbital resolved electronic band structure of the pristine phase, (b) electronic band structure of pristine phase $CsV_3Sb_5$ with and without SOC, (c) orbital resolved electronic band structure of $2 \times 2 \times 1$ CDW phase, and (d) electronic band structure of $2 \times 2 \times 1$ CDW phase.

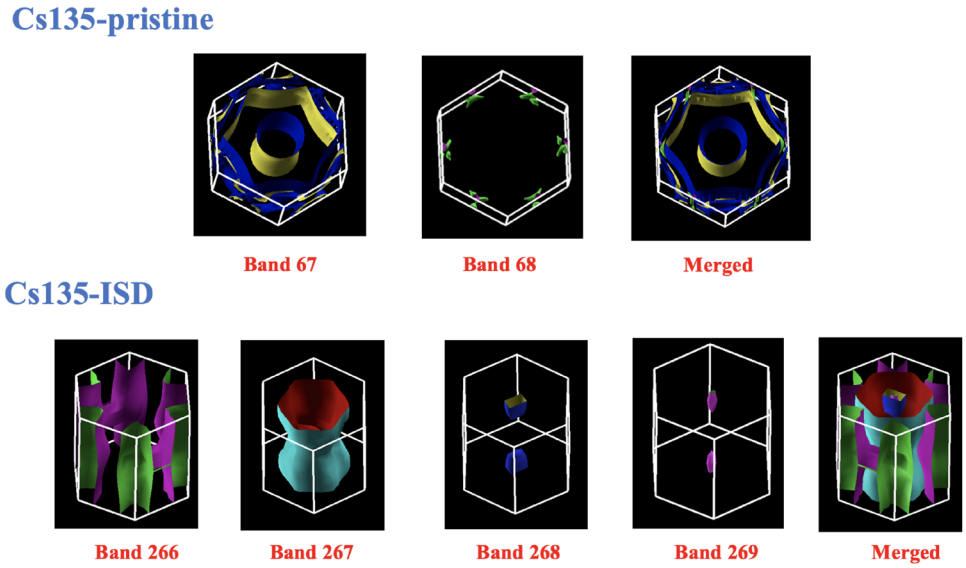


**FIG. 3.** Band-resolved DFT computed Fermi-surfaces of the pristine and $2 \times 2 \times 1$ CDW phases of $CsV_3Sb_5$. A strong 2D characteristic is seen, which has a cylinder-shaped Fermi surface centered near Γ and a large hexagonal Fermi surface in its vicinity in the pristine phase. The significant reconstruction due to distortion is obtained in the Fermi-surface sheet of the CDW phase. The Fermi surface from all bands is displayed in the final picture in both.

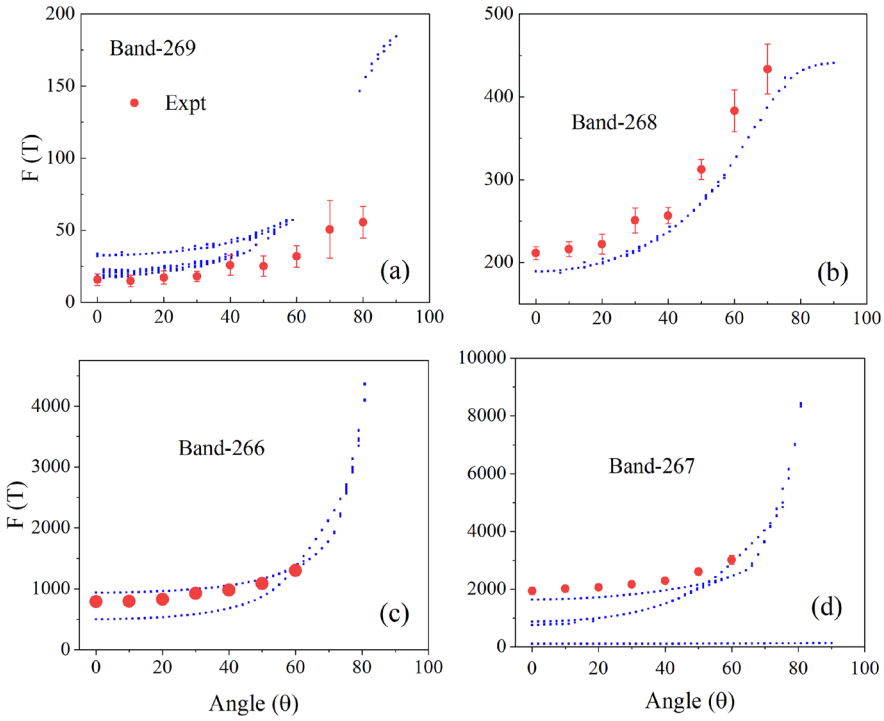


**FIG. 4.** (a)–(d) Comparison between theoretically calculated frequencies with the experimental values at different angles. Theoretical values are calculated using the SKEAF code, and experimental values are adapted from Ref. 8. Theoretical values are in good agreement with the experimental frequencies.

breathing distortion mainly involves the V kagome lattice, the CDW and electron lattice interactions are band selective. Our results regarding the electronic band structure and the Fermi surface are in good agreement with the earlier report.[1,5]

In Fig. 4, we present a comparison between the experimental and calculated angular dependences of the Fermi surface (FS) area for $CsV_3Sb_5$. The experimental data are adapted from Ref. 8. The Onsager relationship[66] was used to convert the theoretical Fermi surface cross-sectional areas into oscillatory frequencies for comparison with the experimental values. As seen from the graph, the theoretically calculated frequencies are in good agreement with the experimental data.

### C. $Z_2$ Invariant calculation

The topological behavior of the materials is called strong or weak based on four $\mathbf{Z}_2$ topological invariants $(\nu_0; \nu_1\nu_2\nu_3)$, which is proposed by Fu-Kane.[67–69] If $\nu_0 = 1$, and other indices $(\nu_1\nu_2\nu_3)$ are equal to zero, the material is classified as strong topological material; if $\nu_0 = 0$ and any of the indices $(\nu_1\nu_2\nu_3)$ is equal to one, it is weak topological material. In the former case, the time reversal symmetry (TRS)-protected surface states are present on all facets, while in the latter case, such surface states are present only on certain facets. The bands that change the $\mathbf{Z}_2$-invariant from trivial to non-trivial or vice versa we call topologically active bands, whereas the ones that do not change $\mathbf{Z}_2$ are called topologically in-active bands. Formally topological activity can be calculated separately for all (even crossing) bands. The change in topological nature, however, only manifests itself in a warped or real gap above the last active band. For the pristine and ISD structure model of $CsV_3Sb_5$, $\mathbf{Z}_2$ invariants were calculated through Fu-Kane indices.[68] This computation was carried out directly from the PW92 band structure, resorting to an approximate Wannier representation. DFT calculations were done with FPLO code using the GGA in the PW92 parameterization. The self-consistent calculations were carried out with spin–orbit coupling (SOC) included. The band structure of the pristine and CDW phases also displays non-trivial band inversion.[1,2] For both cases, we calculated the $\mathbf{Z}_2$ topological invariants and found that both pristine and CDW phases have $(\nu_0; \nu_1\nu_2\nu_3) = (1; 000)$, which is consistent with previous reports.[1,2,5] Hence, the compound $CsV_3Sb_5$ is categorized as being rich with strong topological behavior, providing clear evidence of non-trivial topological band structures.

We confirmed the automatized calculation of these invariants by visual inspection of the Wannier centers as shown in Fig. 5(b). These Wannier centers on $CsV_3Sb_5$ for pristine and CDW phases have been presented for the first time to our knowledge. A clean straight reference line can be drawn for $\theta$ Fig. 5(b), which only crosses this center and hence crosses an odd number of Wannier centers, which results in $\mathbf{Z}_2 = 1$. This and the fact that we can visually connect the Wannier center curves in a reasonably smooth way convince us that the topological indices are 1; (000). For trivial cases, there will be a region around $\theta$ where the reference line passes without crossing or even a number of curves cross in Wannier center curves. Hence, we get 0; (000).

The Wannier centers and reference line for homo 67 for the pristine phase of $CsV_3Sb_5$ are presented in Fig. 5(b) (see Fig. 5 in the supplementary material for the ISD phase). Here, Wannier centers where the last suffix indicates in which plane we are. $z_0$ is a (1/2 1/2 0) plane through the origin in primitive reciprocal basis, while $x_1, y_1$,

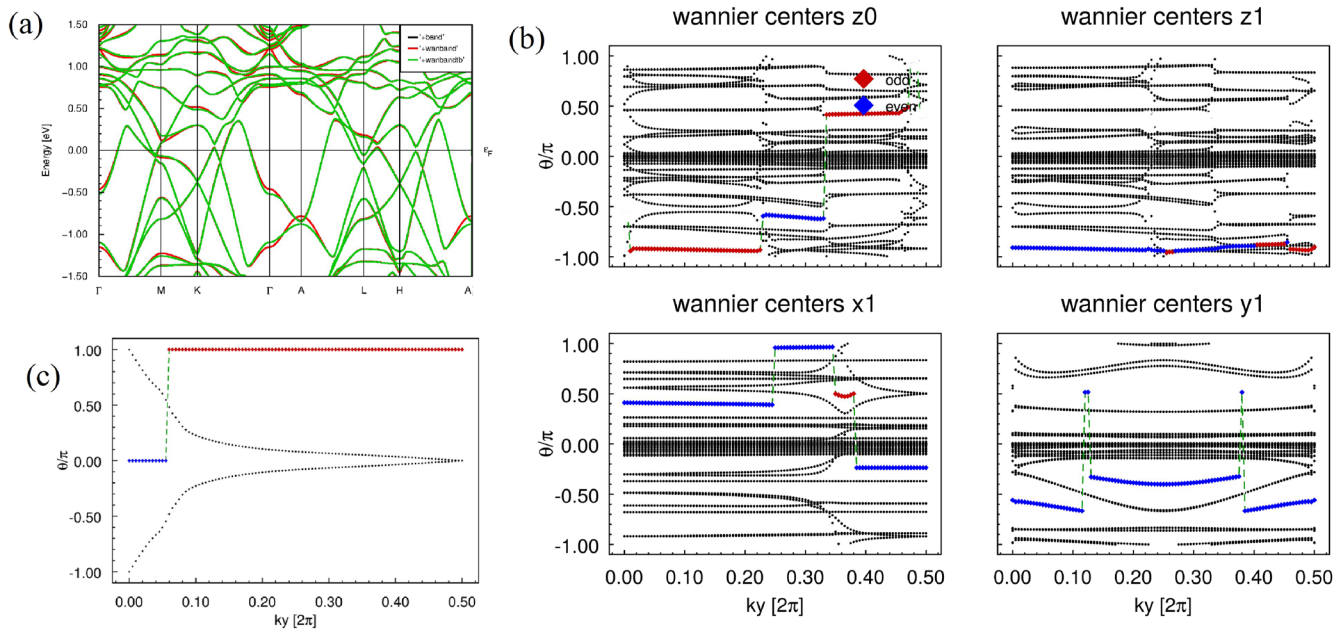


**FIG. 5.** (a) Wannier model bands (red/green) fitted from fplo. (b) Wannier centers and reference line for homo 67. The x1, y1, and z1 planes have zero $\mathbf{Z}_2$ invariant, while plane z0 is non-trivial. (c) Non-trivial $\mathbf{Z}_2$ invariant Wannier center curve representation in the plane spanned by the TRIM.

and $z_1$ denote (0 1/2 1/2), (1/2 0 1/2), and (0 1/2 1/2) planes through (1/2 0 0), (0 1/2 0), and (0 0 1/2).

It can be clearly seen that the $x_1$, $y_1$, and $z_1$ planes have a region ($\theta = 0.5$ or else) where a reference line can pass without any centers crossing in Fig. 5(b), which indicates trivial nature, while in the $z_0$-plane, an odd number of curves cross any reference line [see Fig. 5(c) for reference], which indicates plane $z_0$ is non-trivial. We also confirm this by the algorithm that we use, which has been set as the reference line is printed with blue weights if the number of centers crossed so far is even and in red weights if the number is odd. If the last data point is odd, the invariant is non-trivial. A version of this algorithm[70] is linked directly into FPLO. In the end, we call the invariant odd if a majority of these gap-following curves indicate oddness, as shown in Fig. 5.

## IV. SUMMARY

By means of density functional calculations, we studied the pressure effect of low range pressure on phonon dispersion for both the pristine and CDW phases of $CsV_3Sb_5$. We found that the calculated phonon dispersion relations on the pristine state of $CsV_3Sb_5$ at ambient pressure show two negative energies of the soft acoustic phonon modes at the first Brillouin zone around M and L points, consistent with the previous reports. This structural instability is the cause of the 2 × 2 reconstruction and CDW phase. Interestingly, imaginary phonons appear in the CDW phase at 2 GPa due to structural distortion, which suggests the suppression of the CDW phase. We have also carried out DFT calculations for electronic structures and Fermi surfaces. A strong 2D characteristic is seen, which has a cylinder-shaped Fermi surface centered near Γ and a large hexagonal Fermi surface in its vicinity in the pristine phase. Our DFT calculations confirmed that the Fermi surface of $CsV_3Sb_5$ reconstructs in the CDW phase. From Fu-Kane indices and a version of the algorithm linked directly into FPLO, we calculated $\mathbf{Z}_2$ invariants for both states of $CsV_3Sb_5$. For both cases, we calculated the $\mathbf{Z}_2$ topological invariants and found that both pristine and CDW phases have $(\nu_0; \nu_1\nu_2\nu_3) = (1; 000)$, which is consistent with previous reports. We also confirmed the non-trivial topological band structures by presenting with Wannier center curves. The detailed Fermi surface and $\mathbf{Z}_2$ invariant information for $CsV_3Sb_5$ and the corresponding DFT calculations reported here will be essential to comprehending the superconductivity, charge density wave, and topological phase in $CsV_3Sb_5$ and other $AV_3Sb_5$ family members.

## SUPPLEMENTARY MATERIAL

The supplementary material contains information about the thermodynamical stability via phonon dispersion calculation, band structure and density of states of pristine and 2 × 2 × 2 ISD states of $CsV_3Sb_5$ at different pressures (3–6 GPa) as shown in Figs. 1 and 2.

Figure 3 presents the quality of Wannier fitting with the DFT band 2 × 2 × 2 ISD state of $CsV_3Sb_5$.

The non-trivial $\mathbf{Z}_2$ invariant Wannier center curve for the 2 × 2 × 2 ISD structure of $CsV_3Sb_5$ is shown in Fig. 4. Table I shows the calculated lattice parameters along with the experimental

results for pristine and ISD $CsV_3Sb_5$ in P6/mmm (191) symmetry.

## ACKNOWLEDGMENTS

S.R.B. and D.P.R. thank DST, India, for the ISRF research fellowship (Award No. INSA/DST-ISRF/2022/35). The work at the West Texas A & M University (WTAMU) is supported by the Welch Foundation (Grant No. AE-0025), and the National Science Foundation (Award ID 2336011). The computations were performed on the WTAMU HPC cluster, which was funded by the National Science Foundation (NSF CC* GROWTH 2018841) and IFW Dresden, Germany. We thank Ulrike Nitzsche for her technical assistance.

## AUTHOR DECLARATIONS

### Conflict of Interest

The authors have no conflicts to disclose.

### Author Contributions

**Shalika R. Bhandari**: Conceptualization (equal); Data curation (equal); Formal analysis (equal); Methodology (equal); Validation (equal); Visualization (equal); Writing – original draft (equal); Writing – review & editing (equal). **Mohd Zeeshan**: Conceptualization (equal); Data curation (equal); Formal analysis (equal); Validation (equal); Visualization (equal); Writing – review & editing (equal). **Vivek Gusain**: Conceptualization (equal); Data curation (equal); Formal analysis (equal); Validation (equal); Visualization (equal); Writing – review & editing (equal). **Keshav Shrestha**: Conceptualization (equal); Data curation (equal); Formal analysis (equal); Investigation (equal); Methodology (equal); Project administration (equal); Supervision (equal); Validation (equal); Visualization (equal); Writing – review & editing (equal). **D. P. Rai**: Conceptualization (equal); Data curation (equal); Formal analysis (equal); Investigation (equal); Methodology (equal); Project administration (equal); Software (equal); Validation (equal); Visualization (equal); Writing – review & editing (equal).

## DATA AVAILABILITY

The data that support the findings of this study are available within the article.

## REFERENCES

[1]B. R. Ortiz, L. C. Gomes, J. R. Morey, M. Winiarski, M. Bordelon, J. S. Mangum, I. W. H. Oswald, J. A. Rodriguez-Rivera, J. R. Neilson, S. D. Wilson, E. Ertekin, T. M. McQueen, and E. S. Toberer, Phys. Rev. Mater. **3**, 094407 (2019).
[2]B. R. Ortiz, S. M. L. Teicher, Y. Hu, J. L. Zuo, P. M. Sarte, E. C. Schueller, A. M. M. Abeykoon, M. J. Krogstad, S. Rosenkranz, R. Osborn, R. Seshadri, L. Balents, J. He, and S. D. Wilson, Phys. Rev. Lett. **125**, 247002 (2020).
[3]R. Chapai, M. Leroux, V. Oliviero, D. Vignolles, N. Bruyant, M. Smylie, D. Chung, M. Kanatzidis, W. K. Kwok, J. Mitchell, and U. Welp, Phys. Rev. Lett. **130**, 126401 (2023).
[4]K. Shrestha, V. Marinova, D. Graf, B. Lorenz, and C. W. Chu, Phys. Rev. B **95**, 075102 (2017).
[5]H. Tan, Y. Liu, Z. Wang, and B. Yan, Phys. Rev. Lett. **127**, 046401 (2021).
[6]M. Kang, S. Fang, J. K. Kim, B. R. Ortiz, S. H. Ryu, J. Kim, J. Yoo, G. Sangiovanni, D. Di Sante, B. G. Park, C. Jozwiak, A. Bostwick, E. Rotenberg, E. Kaxiras, S. D. Wilson, J. H. Park, and R. Comin, Nat. Phys. **18**, 301 (2022).
[7]S. Ni, S. Ma, Y. Zhang, J. Yuan, H. Yang, Z. Lu, N. Wang, J. Sun, Z. Zhao, D. Li, S. Liu, H. Zhang, H. Chen, K. Jin, J. Cheng, L. Yu, F. Zhou, X. Dong, J. Hu, H.-J. Gao, and Z. Zhao, Chin. Phys. Lett. **38**, 057403 (2021).
[8]K. Shrestha, R. Chapai, B. K. Pokharel, D. Miertschin, T. Nguyen, X. Zhou, D. Y. Chung, M. G. Kanatzidis, J. F. Mitchell, U. Welp, D. Popović, D. E. Graf, B. Lorenz, and W. K. Kwok, Phys. Rev. B **105**, 024508 (2022).
[9]Y.-P. Lin and R. M. Nandkishore, Phys. Rev. B **104**, 045122 (2021).
[10]C. Setty, H. Hu, L. Chen, and Q. Si, arXiv:2105.15204.
[11]T. Park, M. Ye, and L. Balents, Phys. Rev. B **104**, 035142 (2021).
[12]X. Wu, T. Schwemmer, T. Müller, A. Consiglio, G. Sangiovanni, D. Di Sante, Y. Iqbal, W. Hanke, A. P. Schnyder, M. M. Denner, M. H. Fischer, T. Neupert, and R. Thomale, Phys. Rev. Lett. **127**, 177001 (2021).
[13]J. Zhao, W. Wu, Y. Wang, and S. A. Yang, Phys. Rev. B **103**, L241117 (2021).
[14]E. Uykur, B. R. Ortiz, O. Iakutkina, M. Wenzel, S. D. Wilson, M. Dressel, and A. A. Tsirlin, Phys. Rev. B **104**, 045130 (2021).
[15]F. H. Yu, D. H. Ma, W. Z. Zhuo, S. Q. Liu, X. K. Wen, B. Lei, J. J. Ying, and X. H. Chen, Nat. Commun. **12**, 3645 (2021).
[16]K. Y. Chen, N. N. Wang, Q. W. Yin, Y. H. Gu, K. Jiang, Z. J. Tu, C. S. Gong, Y. Uwatoko, J. P. Sun, H. C. Lei *et al.*, Phys. Rev. Lett. **126**, 247001 (2021).
[17]T. Nguyen, N. Aryal, B. K. Pokharel, L. Harnagea, D. Mierstchin, D. Popović, D. E. Graf, and K. Shrestha, Phys. Rev. B **106**, 075154 (2022).
[18]K. Shrestha, M. Shi, B. Regmi, T. Nguyen, D. Miertschin, K. Fan, L. Z. Deng, N. Aryal, S.-G. Kim, D. E. Graf, X. Chen, and C. W. Chu, Phys. Rev. B **107**, 155128 (2023).
[19]K. Shrestha, D. Miertschin, R. Sankar, B. Lorenz, and C. W. Chu, J. Phys.: Condens. Matter **33**, 335501 (2021).
[20]B. R. Ortiz, P. M. Sarte, E. M. Kenney, M. J. Graf, S. M. L. Teicher, R. Seshadri, and S. D. Wilson, Phys. Rev. Mater. **5**, 034801 (2021).
[21]H. W. S. Arachchige, W. R. Meier, M. Marshall, T. Matsuoka, R. Xue, M. A. McGuire, R. P. Hermann, H. Cao, and D. Mandrus, Phys. Rev. Lett. **129**, 216402 (2022).
[22]N. N. Wang, K. Y. Chen, Q. W. Yin, Y. N. N. Ma, B. Y. Pan, X. Yang, X. Y. Ji, S. L. Wu, P. F. Shan, S. X. Xu *et al.*, Phys. Rev. Res. **3**, 043018 (2021).
[23]F. Du, S. Luo, B. R. Ortiz, Y. Chen, W. Duan, D. Zhang, X. Lu, S. D. Wilson, Y. Song, and H. Yuan, Phys. Rev. B **103**, L220504 (2021).
[24]Z. Liang, X. Hou, F. Zhang, W. Ma, P. Wu, Z. Zhang, F. Yu, J.-J. Ying, K. Jiang, L. Shan, Z. Wang, and X.-H. Chen, Phys. Rev. X **11**, 031026 (2021).
[25]A. A. Tsirlin, P. Fertey, B. R. Ortiz, B. Klis, V. Merkl, M. Dressel, S. D. Wilson, and E. Uykur, arXiv:2105.01397.
[26]H. Chen *et al.*, Nature **559**, 228 (2021).
[27]H. Li *et al.*, Nat. Phys. **18**, 265 (2022).
[28]Y.-X. Jiang, J.-X. Yin, M. M. Denner, N. Shumiya, B. R. Ortiz, G. Xu, Z. Guguchia, J. He, M. S. Hossain, X. Liu *et al.*, Nat. Mater. **20**, 1353 (2021).
[29]S. Cao, C. Xu, H. Fukui *et al.*, Nat. Commun. **14**, 7671 (2023).
[30]X. Teng, L. Chen, F. Ye, E. Rosenberg, Z. Liu, J.-X. Yin, Y.-X. Jiang, J. S. Oh, M. Z. Hasan, K. J. Neubauer, B. Gao, Y. Xie, M. Hashimoto, D. Lu, C. Jozwiak, A. Bostwick, E. Rotenberg, R. J. Birgeneau, J.-H. Chu, M. Yi, and P. Dai, Nature **609**, 490 (2022).
[31]J.-X. Yin, Y.-X. Jiang, X. Teng, M. S. Hossain, S. Mardanya, T.-R. Chang, Z. Ye, G. Xu, M. M. Denner, T. Neupert, B. Lienhard, H.-B. Deng, C. Setty, Q. Si, G. Chang, Z. Guguchia, B. Gao, N. Shumiya, Q. Zhang, T. A. Cochran, D. Multer, M. Yi, P. Dai, and M. Z. Hasan, Phys. Rev. Lett. **129**, 166401 (2022).
[32]H. LaBollita and A. S. Botana, Phys. Rev. B **104**, 205129 (2021).
[33]L. Nie, K. Sun, W. Ma, D. Song, L. Zheng, Z. Liang, P. Wu, F. Yu, J. Li, M. Shan, D. Zhao, S. Li, B. Kang, Z. Wu, Y. Zhou, K. Liu, Z. Xiang, J. Ying, Z. Wang, T. Wu, and X. Chen, Nature **604**, 59 (2022).
[34]C. Mielke III, D. Das, J.-X. Yin, H. Liu, R. Gupta, Y.-X. Jiang, M. Medarde, X. Wu, H. C. Lei, J. Chang, P. Dai, Q. Si, H. Miao, R. Thomale, T. Neupert, Y. Shi, R. Khasanov, M. Z. Hasan, H. Luetkens, and Z. Guguchi, Nature (London) **602**, 245 (2022).
[35]R. E. Peierls, *Quantum Theory Od Solid* (Clarendon Press, Oxford, 1996).
[36]W. Kohn, Phys. Rev. Lett. **2**, 393 (1959).

[37]C. Chen, B. Singh, H. Lin, and V. M. Pereira, Phys. Rev. Lett. **121**, 226602 (2018).
[38]J. van Wezel, P. Nahai-Williamson, and S. S. Saxena, Phys. Rev. B **81**, 165109 (2010).
[39]M. D. Johannes and I. I. Mazin, Phys. Rev. B **77**, 165135 (2008).
[40]A. Y. Liu, Phys. Rev. B **79**, 220515(R) (2009).
[41]X. Zhou, Y. Li, X. Fan, J. Hao, Y. Dai, Z. Wang, Y. Yao, and H.-H. Wen, Phys. Rev. B **104**, L041101 (2021).
[42]C. Wang, S. Liu, H. Jeon, and J.-H. Cho, arXiv:2109.01921.
[43]P. Blaha, K. Schwarz, G. K. H. Madsen, D. Kvasnicka, and J. Luitz, *WIEN2k, An Augmented Plane Wave Plus Local Orbitals Program for Calculating Crystal Properties* (Technische Universiät Wien, Vienna, Austria, 2001), ISBN: 3-9501031-1-2.
[44]K. Koepernik and H. Eschrig, Phys. Rev. B **59**, 1743 (1999).
[45]See https://www.FPLO.de for the FPLO-package (full-potential local-orbital code).
[46]B. Mali, H. S. Nair, T. Heitmann, H. Nhalil, D. Antonio, K. Gofryk, S. R. Bhandari, M. P. Ghimire, and S. Elizabeth, Phys. Rev. B **102**, 014418 (2020).
[47]S. R. Bhandari, D. K. Yadav, B. P. Belbase, M. Zeeshan, B. Sadhukhan, D. P. Rai, R. K. Thapa, G. C. Kaphle, and M. P. Ghimire, RSC Adv. **10**, 16179–16186 (2020).
[48]D. Miertschin, T. Nguyen, S. R. Bhandari, K. Shtefiienko, C. Phillips, B. A. Magar, R. Sankar, D. E. Graf, and K. Shrestha, "Anisotropic quantum transport in ZrSiS probed by high-field torque magnetometry," Phys. Rev. B **110**, 085140 (2024).
[49]G. Kresse and J. Furthmüller, Phys. Rev. B **54**, 11169 (1996).
[50]A. Togo and I. Tanaka, Scr. Mater. **108**, 5 (2015).
[51]J. P. Perdew, K. Burke, and M. Ernzerhof, Phys. Rev. Lett. **77**, 3865 (1996).
[52]E. M. Kenney, B. R. Ortiz, C. Wang, S. D. Wilson, and M. Graf, J. Phys.: Condens.Matter **33**, 235801 (2021).
[53]H. Zhao, H. Li, B. R. Ortiz, S. M. Teicher, T. Park, M. Ye, Z. Wang, L. Balents, S. D. Wilson, and I. Zeljkovic, "Cascade of correlated electron states in a kagome superconductor $CsV_3Sb_5$," arXiv:2103.03118.
[54]J.-F. Zhan, K. Liu, and Z.-Y. Lu, Phys. Rev. B **104**, 195130 (2021).
[55]J.-G. Si, W.-J. Lu, Y.-P. Sun, P.-F. Liu, and B.-T. Wang, Phys. Rev. B **105**, 024517 (2022).
[56]J. A. Wilson, F. J. Di Salvo, and S. Mahajan, Adv. Phys. **24**, 117 (1975).
[57]H. Chen *et al.*, "Roton pair density wave and unconventional strong-coupling superconductivity in a topological kagome metal," arXiv:2103.09188.
[58]Z. Zhang, Z. Chen, Y. Zhou, Y. Yuan, s. wang, J. Wang, H. Yang, C. An, L. Zhang, X. Zhu, Y. Zhou, and Z. yang, Phys. Rev. B **103**, 224531 (2021).
[59]T. Neupert, M. M. Denner, J.-X. Yin, R. Thomale, and M. Z. Hasan, Nat. Phys. **18**, 137 (2022).
[60]M. Wenzel, A. A. Tsirlin, F. Capitani *et al.*, npj Quantum Mater. **8**, 45 (2023).
[61]H. Li, T. T. Zhang, T. Yilmaz *et al.*, Phys. Rev. X **11**, 031050 (2021).
[62]K. Nakayama, Y. Li, T. Kato *et al.*, Phys. Rev. B **104**, L161112 (2021).
[63]Y. Hu, X. Wu, B. R. Ortiz, S. Ju, X. Han, J. Ma, N. C. Plumb, M. Radovic, R. Thomale, S. D. Wilson, A. P. Schnyder, and M. Shi, Nat. Commun. **13**, 2220 (2022).
[64]K. Nakayama, Y. Li, M. Liu, Z. Wang, T. Takahashi, Y. Yao, and T. Sato, Phys. Rev. B **104**, L161112 (2021).
[65]M. I. Naher, F. Parvin, A. K. M. A. Islam, and S. H. Naqib, Eur. Phys. J. B **91**, 289 (2018).
[66]D. Shoenberg, *Magnetic Oscillations in Metals* (Cambridge University Press, Cambridge, 1984).
[67]C. L. Kane and E. J. Mele, Phys. Rev. Lett. **95**, 226801 (2005).
[68]L. Fu and C. L. Kane, Phys. Rev. B **76**, 045302 (2007).
[69]D. J. Thouless, M. Kohmoto, M. P. Nightingale, and M. den Nijs, Phys. Rev. Lett. **49**, 405 (1982).
[70]A. A. Soluyanov, Phys. Rev. B **83**, 235401 (2011); Q. Yin, Z. Tu, C. Gong, Y. Fu, S. Yan, and H. Lei, Chin. Phys. Lett. **38**, 037403 (2021).